Science in China Series G: Physics, Mechanics & Astronomy

www.scichina.com
phys.scichina.com
www.springerlink.com

Calculation of band structure in (101)-biaxially strained Si

SONG JianJun†, ZHANG HeMing, HU HuiYong & FU Qiang

Key Laboratory of Ministry of Education for Wide Band-Gap Semiconductor Materials and Devices, School of Microelectronics, Xidian University, Xi'an 710071, China

The structure model used for calculation was defined according to Vegard's rule and Hooke's law. Calculations were performed on the electronic structures of (101)-biaxially strained Si on relaxed $Si_{1-X}Ge_X$ alloy with Ge fraction ranging from $X = 0$ to 0.4 in steps of 0.1 by CASTEP approach. It was found that [±100] and [00±1] valleys (Δ_4) splitting from the [0±10] valley (Δ_2) constitute the conduction band (CB) edge, that valence band (VB) edge degeneracy is partially lifted and that the electron mass is unaltered under strain while the hole mass decreases in the [100] and [010] directions. In addition, the fitted dependences of CB splitting energy, VB splitting energy and indirect bandgap on X are all linear.

strained Si, band structure, effective mass

Strained silicon (S-Si) technology is one of the most advanced technologies in nowadays microelectronics. It has the advantages of high-mobility, adjustable energy-band structure and compatible processing technology with traditional silicon[1]. Up to now, numbers of hetero-junction devices and circuits of S-Si have been put into practical use[2]. Band structure is the essential of fully understanding and investigating the properties of material[3]. However, few theoretical researches on band structure under strain were found, especially (101)-biaxial strain. Many results were referenced directly in a great amount of researches concerning the design of new device structures based on strained Si[4]. So it is necessary to study the band structure of (101)-biaxially S-Si.

The band structure of S-Si can be obtained by various approaches: the pseudopotential method, the linear coupled atomical orbital (LCAO) method, the free-electron approximation method, and the k.p perturbation method (sometimes referred to as the effective-mass method). In terms of convenience and accuracy, we will investigate the band structure of (101)-biaxially S-Si using CASTEP (CAmbride Serial Total Energy Package) approach, first-principles simulations calculated from density-functional theory with plane waves and pseudopotentials[5]. The calculation results are in good accordance with k.p theoretical calculation[6,7].

1 The structure model

Since CASTEP can only be used to perform calculations on 3D periodic structure, whether strained film has 3D periodic structure is of interest. In the plane of the interface between the film and its substrate, the film is forced to adopt the lattice structure of its host substrate. So lattice periodicity is preserved under such strain and CASTEP calculation on S-Si film is valid.

The structure used to calculate must be specified firstly. In order to prepare the structure of S-Si, we import a Si convention cell structure from an existing structure file, and then create a Si supercell structure with modified lattice parameters (shown in Figure 1).

Modification of lattice parameters is achieved by the following formulae:

Received August 31, 2007; accepted December 11, 2008
doi: 10.1007/s11433-009-0078-1
†Corresponding author (email: wmshhsong@tom.com)
Supported by the National Pre-research Foundation of China (Grant Nos. 51308040203 and 51408061105DZ0171)

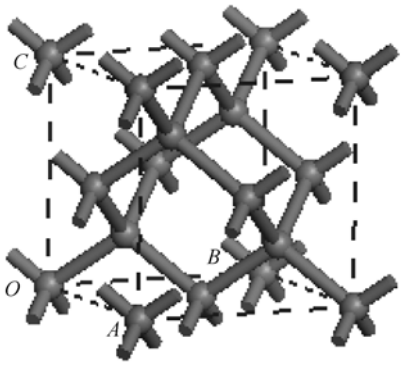

Figure 1 Schematic supercell structure of strained silicon, where $OA=a$, $OB=b$, $OC=c$; $\angle AOB=\gamma$, $\angle AOC=\beta$, $\angle BOC=\alpha$.

$$\begin{bmatrix} a \\ b \\ c \end{bmatrix} = \begin{bmatrix} \varepsilon_{xx} & \varepsilon_{xy} & \varepsilon_{xz} \\ \varepsilon_{yx} & \varepsilon_{yy} & \varepsilon_{yz} \\ \varepsilon_{zx} & \varepsilon_{zy} & \varepsilon_{zz} \end{bmatrix} \cdot \begin{bmatrix} a_0 \\ a_0 \\ a_0 \end{bmatrix} + \begin{bmatrix} a_0 \\ a_0 \\ a_0 \end{bmatrix}, \quad (1)$$

$$\begin{aligned} &\arccos(\varepsilon_{yz}) = \alpha, \arccos(\varepsilon_{xz}) = \beta, \\ &\arccos(\varepsilon_{xy}) = \gamma, \end{aligned} \quad (2)$$

where symbol a_0 is Si lattice constant and the strain tensor is determined according to Vegard's rule and Hooke's law. The formulae of the strain tensor are as follows[8]. Values of parameters used in calculation are listed in Table 1. The results of the modified lattice parameters are listed in Table 2.

$$\varepsilon_{\parallel} = (a_{\mathrm{Si}_{1-x}Ge_x} - a_{\mathrm{Si}})/a_{\mathrm{Si}}, \quad (3)$$

$$\begin{aligned} &\varepsilon_{xx} = \varepsilon_{zz} = 1/2[1-1/\sigma^{(101)}]\varepsilon_{\parallel}, \\ &\varepsilon_{xy} = -1/2[1+1/\sigma^{(101)}]\varepsilon_{\parallel}, \\ &\varepsilon_{yz} = \varepsilon_{zx} = 0, \quad \varepsilon_{yy} = \varepsilon_{\parallel}. \end{aligned} \quad (4)$$

Table 1 Values[9] of parameters used in calculation

Parameter	Symbol (unit)	Value
Si lattice constant	a_0 (Å)	5.4309
Ge lattice constant	a_0 (Å)	5.6579
Possion's ratio	$\sigma^{(101)}$	1.959

Table 2 Values of S-Si lattice parameters

X	a (Å)	b (Å)	c (Å)	$\alpha=\gamma$ (°)	β (°)
0.1	5.429	5.433	5.429	90	90.18
0.2	5.427	5.439	5.427	90	90.36
0.3	5.425	5.444	5.425	90	90.54
0.4	5.423	5.448	5.423	90	90.72

2 Calculation setup

Once suitable 3D periodic structure has been defined, it is necessary to set the parameters associated with the calculation task[10]. In this work, the exchange correlation potential in the local density approximation (LDA) for electron-electron interaction is adopted. The typical configuration for Si is $3s^2 3p^2$. Integrations in the Brillouin Zone (BZ) are performed using special k points generated with a 5×5×5 mesh parameter grid. One electron valence states are expanded in a basis of plane waves with a cutoff energy of 180 eV. Such parameters have been tested to be sufficient for convergence. We then use the strained structure for energy band calculation.

3 Analysis of the band structure

The effects of strain on the band structure are considered in this section. Band structures of unstrained Si and strained Si on (101) relaxed $Si_X Ge_{1-X}$ with Ge fraction ranging from $X=0.1$ to 0.4 in steps of 0.1 by CASTEP approach are presented graphically in Figures 2—6.

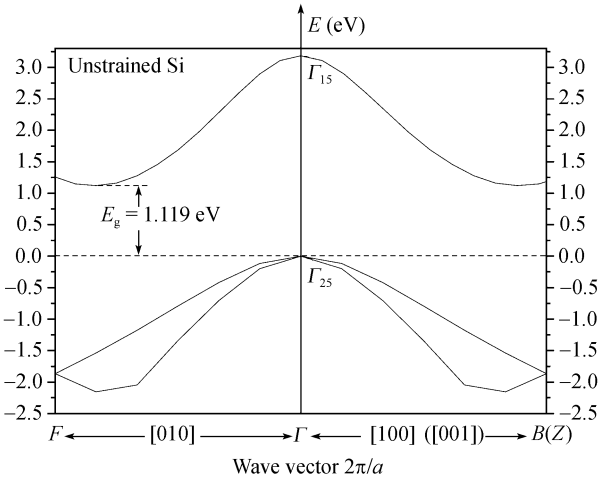

Figure 2 The $E(k)$ relation for unstrained Si.

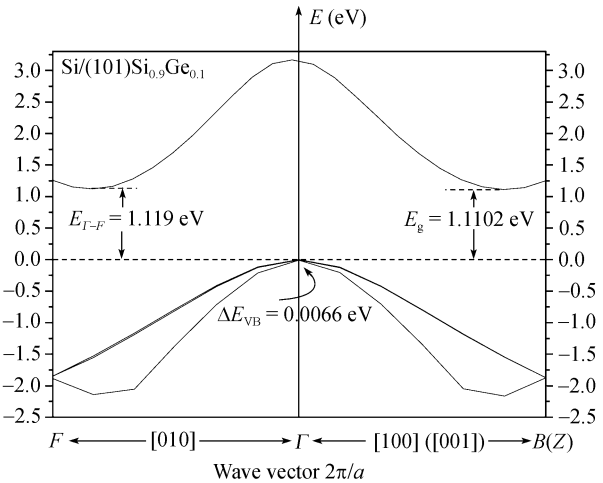

Figure 3 The $E(k)$ relation for $Si/(101)Si_{0.9}Ge_{0.1}$. The notation is as follows: $E_{\Gamma-F}$, the [0±10] valley; E_g, the [±100] and [00±1] valleys; ΔE_{VB}, the valence band splitting between upper and lower bands.

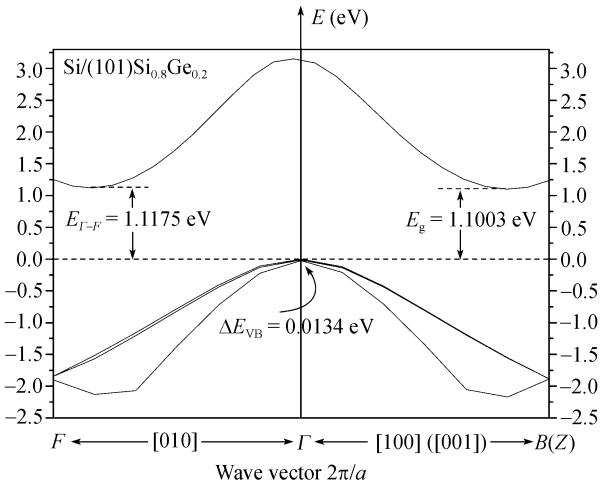

Figure 4 As in Figure 3, but for Si/(101)$Si_{0.8}Ge_{0.2}$.

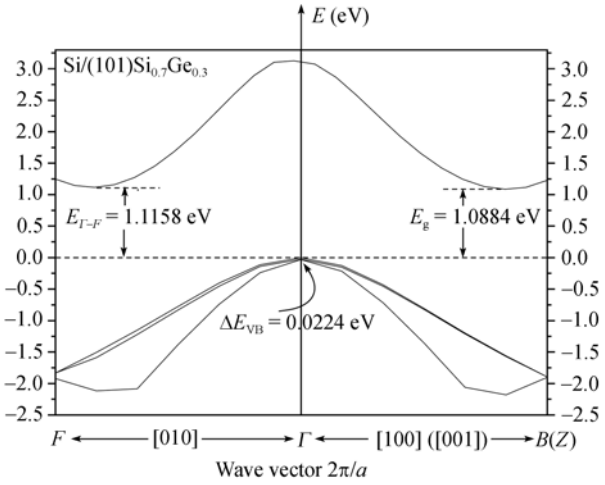

Figure 5 As in Figure 3, but for Si/(101)$Si_{0.7}Ge_{0.3}$.

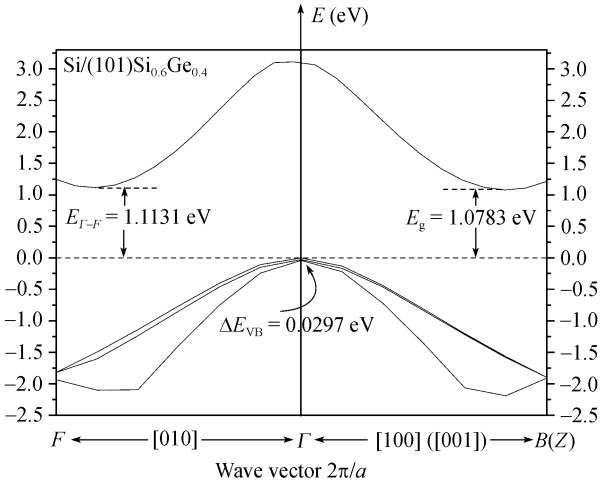

Figure 6 As in Figure 3, but for Si/(101)$Si_{0.6}Ge_{0.4}$.

Analysis of Figures 2—6 indicates

1) Growth on a substrate of (101) orientation produces a monoclinic distortion and splits the six Δ levels. The [±100] and [00±1] valleys (Δ_4) splitting from the [0±10] valley (Δ_2) constitute the CB edge, and the CB edge decreases in energy with increasing Ge fraction X (shown in Figure 10). The CB splitting energy between Δ_4 and Δ_2 valleys extracted from Figures 2—6 is fitted as a function of X. The result is plotted in Figure 7.

2) The effect of partially lifting the VB edge degeneracy is clearly shown in all cases. The VB edge is characterized by the upper band. The valence band splitting energy between upper and lower bands at $k=0$ extracted from Figures 2—6 is fitted as a function of X. The result is shown in Figure 8.

3) The decrease in indirect bandgap with increasing X is shown in Figure 9. It is notable that no results of VB splitting and indirect bandgap from other references have been found, and hence, our data remain undetermined.

Now turn to effective mass of strained films on (101)

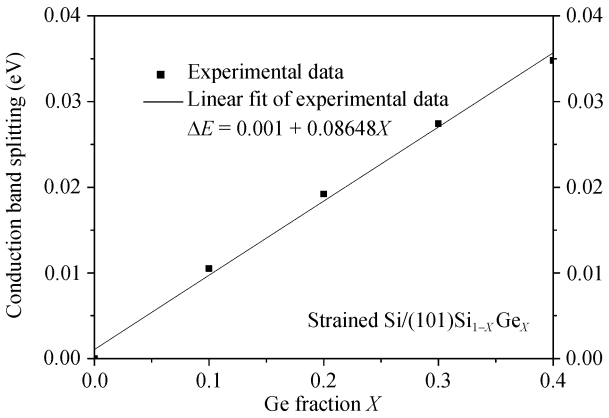

Figure 7 The conduction band splitting between Δ_4 and Δ_2 valleys versus X in strained Si/(101)$Si_{1-X}Ge_X$.

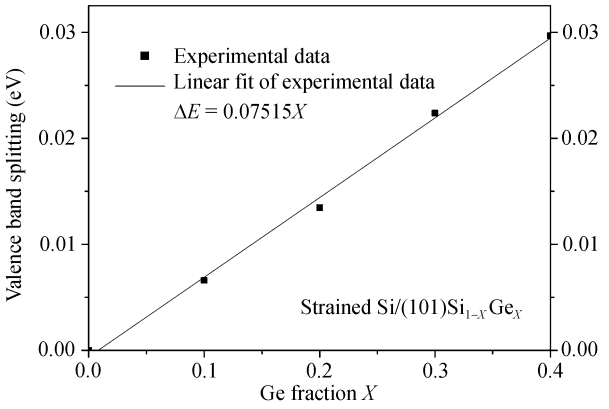

Figure 8 The valence band splitting between upper and lower bands versus X at $k=0$ in strained Si/(101)$Si_{1-X}Ge_X$.

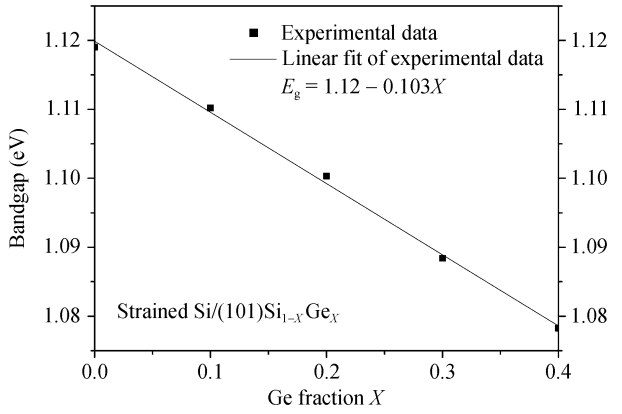

Figure 9 Extracted values of indirect bandgap versus X in strained Si/(101)$Si_{1-X}Ge_X$.

substrate. As shown in Figure 10, the shape of the energy valleys described by electron mass of CB is unaltered under strain. Figure 11 shows that the shape near the energy maximum described by hole mass of VB changes regularly with the increase of X. Planar isotropic tensile strain slightly decreases the hole mass in the [100] and [010] directions. The above results are explained by the following facts:

1) Through varying k in the vicinity of energy valleys, the deformation potential fields are taken as constant. Therefore, all points near energy valleys shift by the same account. In addition, the CB states without strain which are degenerate in energy have significantly different wavevectors. So, for any specific wavevector, no pair of CB states under strain is degenerate or very close in energy. This means that any coupling between them is insignificant, and therefore may be neglected. Thus, the shapes of the energy valleys in CB are preserved.

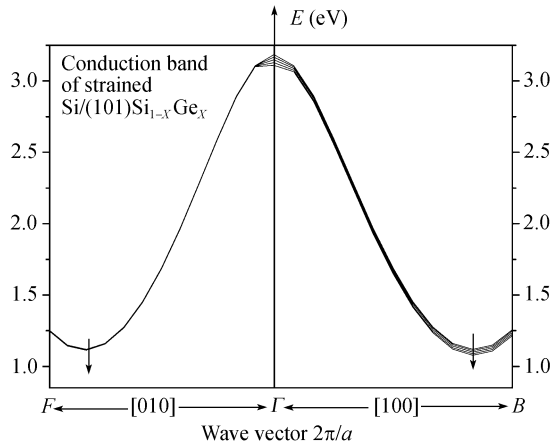

Figure 10 Strain effect on the conduction band of Si/(101) $Si_{1-X}Ge_X$. The arrows indicate the increase of Ge fraction from $X=0$ to 0.4 in steps of 0.1.

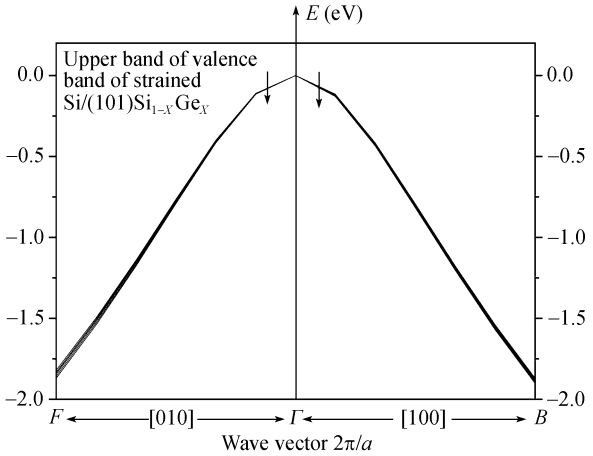

Figure 11 Strain effect on the upper band of valence band of Si/(101) $Si_{1-X}Ge_X$. The arrows indicate the increase of Ge fraction from $X=0$ to $X=0.4$ in steps of 0.1.

2) In contrast to the CB, although the deformation potentials are independent of wavevector for points in the vicinity of the center of the BZ, the states of the VB, whose wavevectors lie near the center of the BZ, will be either degenerate or very close to one another in energy, and so, are coupled to one another. Thus, a change in the shape near the energy maximum in VB occurs.

4 Conclusion

Calculations were performed on the electronic structures of (101)-biaxially strained Si on relaxed $Si_{1-X}Ge_X$ alloy with Ge fraction ranging from $X=0$ to 0.4 in steps of 0.1 by CASTEP approach. By analysis of the band structure charts obtained, we found a decrease in indirect bandgap and an increase in CB, VB edge splitting energy with increasing X. Moreover, the shape of the energy valleys described by electron mass of CB is unaltered under strain while the shape near the energy maximum described by hole mass of VB changes regularly with increasing X. Planar isotropic tensile strain slightly decreases the hole mass in the [100] and [010] directions.

1 Hu H Y, Zhang H M, Jia X Z, et al. Study on Si-SiGe three-dimension CMOS integrant circuits. Chin J Semiconduct, 2007, 28(5): 36－40

2 Watling J R, Yang L, Borici M, et al. The impact of interface roughness scattering and degeneracy in relaxed and strained Si n-channel MOSFETs. Solid-State Electron, 2004, 48: 1337－1346

3 Chattopadhyay S, Driscoll L D, Kwa K S K, et al. Strained Si MOSFETs on relaxed SiGe platforms: Performance and challenges.

Solid-State Electron, 2004, 48: 1407－1416
4 Guillaume T, Mouis M. Calculations of hole mass in [110]-uniaxially strained silicon for the stress-engineering of p-MOS transistors. Solid-State Electron, 2006, 50: 701－708
5 Chen Z W, Lv M Y, Liu R P. Stability and electronic structure of ordered $Si_{0.75}Ge_{0.25}C$ alloy. J Appl Phys, 2005, 98: 1－3
6 Rieger M M, Vogl P. Electronic-band parameters in strained $Si_{1-x}Ge_x$ alloys on $Si_{1-y}Ge_y$ substrates. Phys Rev, 1993, 48(19): 276－287
7 Dhar S, Kosina H, Palankovski V, et al. Electron mobility model for strained-Si devices. IEEE Trans Electron Devices, 2005, 52(4): 527－533
8 Smirnov S, Kosina H. Monte Carlo modeling of the electron mobility in strained $Si_{1-x}Ge_x$ layers on arbitrarily oriented $Si_{1-y}Ge_y$ substrates. Solid-State Electron, 2004, 48: 1325－1335
9 Fischetti M V, Laux S E. Band structure, deformation potential, and carrier mobility in strained Si, Ge and SiGe alloy. J Appl Phys, 1996, 80(4): 2234－2252
10 Li Y, Liu Y, Chen N, et al. Vacancy and copper-doping effect on superconductivity for clathrate materials. Phys Lett A, 2005, 345: 398－408